Bubble Detection with Semantic Segmentation for Multiphase Flow Particle Image Velocimetry

Walisson Chaves Ferreira Pinto
Pontifical Catholic University of Rio de Janeiro
Rio de Janeiro, Brazil
walisson.chaves@gmail.com

Antônio M. Pinto
Pontifical Catholic University of Rio de Janeiro
Rio de Janeiro, Brazil
antoniomoreira@aluno.puc-rio.br

Paulo Rodrigo Cavalin
IBM Research
Rio de Janeiro, Brazil
pcavalin@br.ibm.com

David Menotti
Federal University of Parana (UFPR)
Curitiba, Brazil
menotti@ufpr.br

Igor Braga de Paula
Pontifical Catholic University of Rio de Janeiro
Rio de Janeiro, Brazil
igordepaula@puc-rio.br

Helon Vicente Hultmann Ayala
Pontifical Catholic University of Rio de Janeiro
Rio de Janeiro, Brazil
helon@puc-rio.br

***Abstract*—In this paper, we present an evaluation of semantic segmentation for bubble detection in multiphase flow particle image velocimetry (PIV), from which a lot of applications in oil, gas, and chemical industries, for instance, can benefit. The problem is challenging, however, given the differences in contrast that can make the bubble almost invisible at blind eye. Thus, for this research we have collected and manually annotated a dataset with 1161 images, and trained a U-Net neural network to perform the detection of the bubbles. The experiments presented pixel accuracies of about 86.78% on the largest test set, with more challenging images, but more than 99% can be achieved with more training images and less test images. We believe that, although preliminary, the results are encouraging towards the development of a fully-automated Computer Vision-based system for PIV, but more effort should be put into expanding the training set and enhancing the evaluation protocol in future work.**

***Index Terms*—Particle image velocimetry, Semantic segmentation, Taylor bubble, Machine learning, Deep learning**

I. Introduction

Various nonstationary two-phase bubbly flows are often found in the oil, gas, chemical, nuclear, and aerospace industries having abundant applications [1]. Probe-based (contact) and non-invasive (non-contact) methods are the two main classes of measurement techniques for two-phase flow diagnostics. In the former it is possible to evaluate physical quantities such as temperature, pressure, or velocity at high frequency in a given flow region and, thus, derive its average and fluctuating values. The later has the advantage of not disturbing the flow under investigation, being most of the optical approaches, which have been significantly accelerated along with the evolution of laser, engraving, and computer technologies [2].

Even though probe-based approaches are usually the most precise set of tools to achieve high precision in terms of measurement, they also tend to be more expensive and difficult to scale up to larger sets of flows. Non-invasive methods, on the other hand, might not reach the quality of the others in terms of quality, but recent advances in Computer Vision (CV) are encouraging towards defining approaches that are good enough for practical applications involving bubly flows.

One of such applications is Particle Image Velocimetry (PIV), a well-developed and contactless technique in experimental fluid mechanics. It consists of a measurement technique that allows for capturing velocity information of whole flow fields in fractions of a second [3]. Furthermore, the strong velocity gradient and streamline curvature near the wall substantially limit its accuracy improvement [4]. One important step for this application is a precise detection of the bubles, from which speed can be calculated from the difference between two subsequent timeframes. But that task is very challeging, especially due to the dispersion of the laser light caused by the gas-liquid interfaces [5]. The boundaries of the buble vary considerably in terms of contrast to the fluid background, which makes the segmentation task more difficult and requires an approach that is adaptive at pixel level.

Modern non-intrusive experimental detection techniques including electrical capacitance tomography (ECT), electromagnetic tomography (EMT), computed tomography (CT), PIV, particle tracking velocimetry (PTV), have been widely applied for the study of flow and transport phenomena with the aid of machine learning (ML), especially deep learning (DL), as these techniques are able to process images more accurately and efficiently in problems of classification, object detection,

This study was financed in part by the Coordenação de Aperfeiçoamento de Pessoal de Nível Superior - Brasil (CAPES) - Finance Code 001, and by Fundação Carlos Chagas Filho de Amparo à Pesquisa do Estado do Rio de Janeiro – FAPERJ

segmentation, reconstruction and noise removal if compared to traditional techniques [6].

In this context, machine learning has been succesfully applied to fluid mechanics problems. In [7], the authors propose a deblur filter using a generative adversarial network (GAN) was developed and applied to real PIV images. The authors found that the deblurred images resulted in less PIV velocity error by applying the generator to actual experimental images of a synthetic jet. Authors of [8] presented a study concerning a combined sonic-hotfilm anemometer, and a fully automated in situ calibration procedure implementing DL. The calibration procedure was tested on both the open sea dataset and inside a wind tunnel, it has shown to have the robustness necessary for operation in everchanging open field flow and environmental conditions. In [9], the authors implemented genetic programming on an experimental setup in order to improve flow control performance for bluff bodies wakes.

Machine learning has been applied to understaning bubble dynamics and for the detection of their characteristics such as their location, shape, diameters and speeds. In [10], the authors presented a deep learning based approach to detect underwater bubbles, where the real-time object detector YOLO [11] framework has been adapted for this task. In [12], the authors applied the principal component analysis (PCA) technique to extract physical descriptors of pool boiling experimental images. The dominant frequency and amplitude of the time-series principal components were used as new physical descriptors to distinguish different boiling regimes. They used a bidirectional long short-term memory (BiLSTM) neural network to estimate the future variations of PCs and hence the bubble dynamics to predict future boiling states, so that boiling crises can be detected. The proposed approach was able to predict reduced-order bubble images well. The authors of [13] trained the instance segmentation Mask R-CNN to develop an automated bubble detection and mask extraction tool applicable to a varity of two-phase flows. The dataset used included experimental images of bubbly flows and realistic synthetic bubble images. In the training process the loss function was weighted according to bubble size. The proposed model showed to be accurate under a wide range of experimental conditions.

In [14], the authors introduced three bubble velocimetry methods, inclunding a fine-tuned CNN-based model, which was re-trained using the synthetic bubble images. The proposed method correctly measure the temporal variation of the bubble velocity when compared with the traditional PTV method. In [15], the authors try to handle different image conditions, higher gas volume fractions and a proper reconstruction of the hidden segment of a partly occluded bubble in the task of identifing and segmenting bubbles. The authors tested three different methods based on CNN's. The Mask R-CNN performed equally good compared to the StarDist method, which was initially developed for segmenting cell nuclei in biomedical images.

Characterizing velocity field measurements in flows that present Taylor bubbles is important to understand the underlying mechanisms of such phenomenom that spans diverse applications such as oil, nuclear, chemical industries [16]. However, doing so currently requires that engineers label manually bubbles in many images, which is expensive, tedious and error prone. As most PIV methods are based on time-shifted image correlation, it is important to segment the input images so that the bubbles are removed in a pre-processing stage, as it influences the overall result and the final analysis. In this context, the main goal of the present work is to evaluate the applicability of state-of-the-art neural networks for semantic image segmentation, applied to the problem of Taylor bubble detection in multiphase flow. For that end, we evaluate the U-Net neural network on a set of 1161 images collected for this paper, captured from 5 different PIV experiments, using different hold-out dataset splits ranging from 20 to 40%, in order to asses how the model would generalize on images from unseen experiments. The results point out accuracies ranging from 86.78% to 99.81% of pixel accuracy, with less and more training images, respectively. The quality of the results presented impact directly the methodology for PIV in bubbly flows and will enable practitioners to adopt such a tool in their analysis procedure, avoiding time spent on tedious tasks and providing more accurate results.

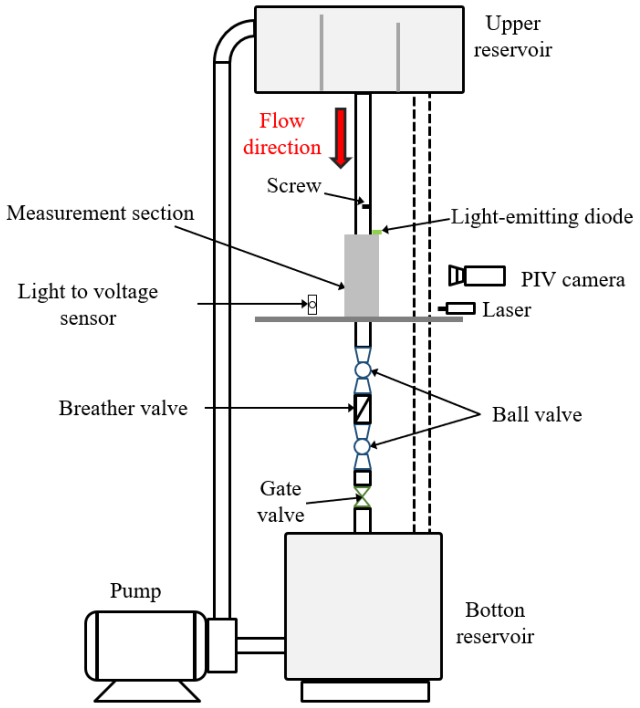

Fig. 1. Schematic layout of the experimental facility.

The rest of the paper is organized as follows. The case study is presented in Section II. Section III presents the methodology used in this work. In Section IV the results are presented, finally Section V presents the conclusions and future works.

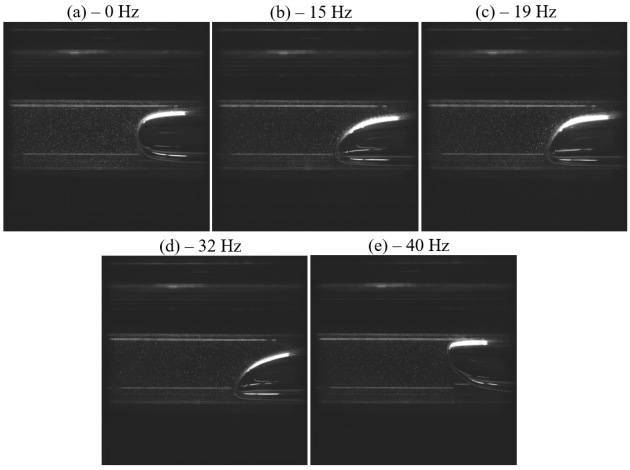

Fig. 2. Bubble shapes for each flow condition.

II. Case study

The experiments described in this section investigate the motion and the shape of Taylor bubbles rising in vertical pipes against downward liquid flows. Figure 1 shows the schematic layout of the experimental facility. The upper reservoir has dimensions of 0.65 m x 0.275 x 0.220 m and is made of acrylic. It has two inner plates used to maintain a uniform water column above the pipe, and consequently maintain a constant pressure. The left plate is 0.215 m high and the right one is 0.205 m high. The excess water that overflows over the second plate is drained by a tube back to the lower reservoir to be pumped to the top again. The experiment is conducted in a turbulent regime, as for the laminar case a much larger pipeline would be required, but this would be unfeasible considering the available environment. The smallest Reynolds number used in the experiment was 3178.

In the measurement section, an acrylic box (0.12 m x 0.095 m x 0.22 m) was used around the tube in order to reduce optical distortion. A 29.5 mm long screw was installed to fix the Taylor bubble in a radial position. A honeycomb was used right at the entrance of the pipe in order to align the flow and avoid vortices. A white LED panel behind the acrylic box in order to improve the visualization of the bubble contour. Polyamide tracer particles with a diameter of 50 μm were added to the water to make it possible to use the PIV method. The camera used in the experiments has a resolution of 1280 x 1024 pixels.

Water flowed up to the topmost section through the vertical pipe. A valve system was used to generate the Taylor bubble. First, the upper valve is closed, interrupting the flow of water. With the two lower valves open, the breather valve is opened until the volume of air inside the tube reaches a volume of 100 cm^3.

The tests were performed in five different configurations. For each test, a desired flow rate was chosen using the gate valve and a multimeter that allows its visualization in hertz, later transformed into m^3/s. The settings chosen were: stagnant flow (0 Hz), 15 Hz, 19 Hz, 32 Hz, and 40 Hz. In the case of the 40 Hz flow rate, it was not possible to manually perform a subtle transition from a lower flow rate to the desired one between the inserted screw and the laser position, which generated instability in the bubble, preventing the acquisition of images in the proper position. For this reason, the images obtained by these tests are in the opposite position to the previous flows.

Figure 2 shows an example of a bubble for each configuration mentioned. It is possible to observe that the symmetry of the bubble is already broken at 15 Hz.

III. Methodology

In this section we present a brief introduction to semantic segmentation, then we describe how it has been implemented and the evaluation metrics used in this work.

A. Semantic segmentation

Semantic segmentation is an important research topic in computer vision along with object detection and image classification. In a semantic segmentation task, a label is assigned to each pixel, thus, an image is partitioned into semantically meaningful coherent regions. It comprises image classification, object detection and boundary location, which makes it a challenging task [17]–[19]. Figure 3 shows an example of object detection (a), and classification of each pixel (b) into different classes (plantation, sky, tree, florest, bush, and person).

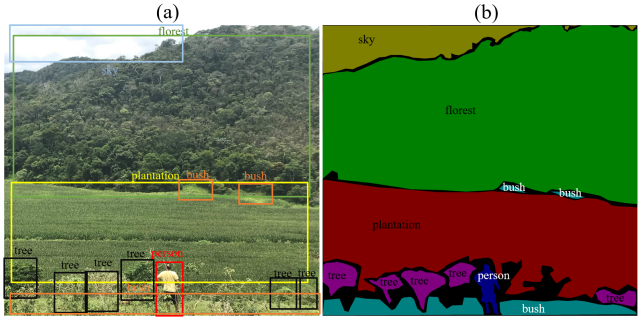

Fig. 3. Example of object detection and semantic segmentation.

One widely adopted method for semantic segmentation is U-Net [20], consisting of an encoder-decoder neural network archicture divided in two stages, i.e. one to encode the input image into a semantic representation, and another one to decode that representation and generate an output image with the respective semantic classes for each pixel. The main challenges lies with in properly setting up a set of images to train the network, to understand how it performs on the buble detection problem. Further details about this method are presented next.

B. Proposed method

In order to perform the segmentation of bubbles in multiphase flow through PIV images, a neural network with a encoder-decoder structure is proposed, based on the U-Net

architecture [20]. The network is composed of two parts, as shown in Figure 4. The structure on the left side (encoder) is responsible for the feature extraction process. The right side of the network (decoder) establishes a feature map restoration model. The proposed model also densely connects all feature maps in the down-sampling stage, as proposed by [20].

The network consisted of two 2×2 convolutional layers followed by batch normalization (BN), and ReLU activation function in each block. In the contracting path, the number of filters in each block was increased by a factor of 2, starting from 64 filters in the first block to 1024 filters in the last block, with 2 pixel-window max-pooling layers between blocks. In the expanding path the last 1 layer were has sigmoid as the activation function. The whole network has 31,054,145 parameters in total, from which 31,042,369 are trainable. The architecture of the U-Net is shown by Figure 4.

C. Evaluation Metrics

The performance of the algorithms was assessed by calculating four evaluation metrics, namely *Pixel Accuracy (PA)*, *Balanced Pixel Accuracy (BPA)*, *Intersection over Union (IoU)*, and the *Dice Similarity Coefficient (DSC)*. Since the classes in the images are unbalanced, the PA should be evaluated with other supporting evaluation metrics in this case. In this way, the three other metrics take into account that the dataset ist not balanced, and also the overlap between the ground truth and model prediction. The value of $MeanIoU$ varies between 0% and 100%, respectively, for no overlap and complete overlap between two regions. The *DSC* varies between 0 and 1, following the same idea as the previous metric.

1) Pixel Accuracy: The *Pixel Accuracy (PA)* is the percent of pixels in the image that are classified correctly. It simply calculates the ratio between the amount of adequately classified pixels and the total number of pixels in the image, as shown by (1)

$$PA = \frac{\sum_{j=1}^{k} n_{jj}}{\sum_{j=1}^{k} t_j} \tag{1}$$

where n_{jj} represents the total number of pixels both classified and labeled as class j, and t_j is the total number of pixels labeled as class j.

2) Balanced Pixel Accuracy: The *Balanced Pixel Accuracy (BPA)* computes the balanced *PA* in order to avoid inflated performance estimates on imbalanced datasets. In the binary case, the *BPA* is equal to the arithmetic mean of sensitivity and specificity

$$BPA = \frac{1}{2}\left(\frac{TP}{TP+FN} + \frac{TN}{TN+FP}\right) \tag{2}$$

where *TP* is number of true positives, *TN* is the number of true negatives, *FP* are the false positives, and *FN* are the false negatives.

3) Intersection over Union: Intersection over Union (IoU) is essentially a metric to quantify the percent overlap between the ground truth and the prediction of the model.

$$IoU(A,B) = \frac{|A \cap B|}{|A \cup B|} \tag{3}$$

where $|A \cap B|$ is the area of overlap, and $|A \cup B|$ is the area of union.

4) Dice Similarity Coefficient: The *Dice Similarity Coefficient (DSC)* measures the spatial overlap between two segmentations.

$$DSC = \frac{2 * |A \cap B|}{|A| + |B|} \tag{4}$$

where $|A|$ represents the total of pixels in the ground truth and $|B|$ in the prediction of the model.

IV. Results

All tests were performed on a server that has multiple CPUs and GPUs such as NVIDIA Tesla P100 and AMD EPYC 7352 24-Core Processor. The proposed model was implemented with TensorFlow v2.9.2, with the use of Keras library. We adopted a basic U-Net architecture framework with four blocks in the contracting and expanding paths as described in Section III. We used the Adaptive Moment Estimation (ADAM) as optimizer with learning rate (LR) of 10^{-2}. We replaced the cross-entropy loss function from the configuration described by [20] with the Dice coefficient loss. We use early stopping in all cases and the models are trained for up to 100 epochs.

Particle image velocimetry data were collected in laboratory. There are a total of 1161 images that have dimensions of 1000x1016 pixels. The images were resized to 256x256 pixels to train the neural network from scratch. All annotations were performed using LabelMe[1], which is an open graphical annotation tool.

Five tests were performed for three holdout percentages as shown by Table I. We quantitatively evaluate the performance of the proposed U-Net using the four complementary evaluation metrics descriped in the previous section. Table I illustrates the performance of our U-Net trained to segment bubbles in multiphase flow of PIV images. According to Table I, the average pixel accuracy ranges from 86.78% to 99.81%, for a percentage of 40% and 20%, respectively.

Although the average pixel accuracy for a 40% holdout is 86.78%, the balanced value drops considerably for this holdout percentage, and the average value of the Mean IoU and the Dice coefficient are only 64.09% and 0.569, respectively. It is possible to observe, however, that the standard deviation is high, indicating that some of the tests have reasonable performance. This is shown in Figure 5, where a visual inspection of predictions from two test images has been done. The network trained in test image #3 has low ability for the segmentation task. The model is able to classify only part of the region containing particles, and it is not able to identify and

[1] http://labelme.csail.mit.edu/Release3.0/

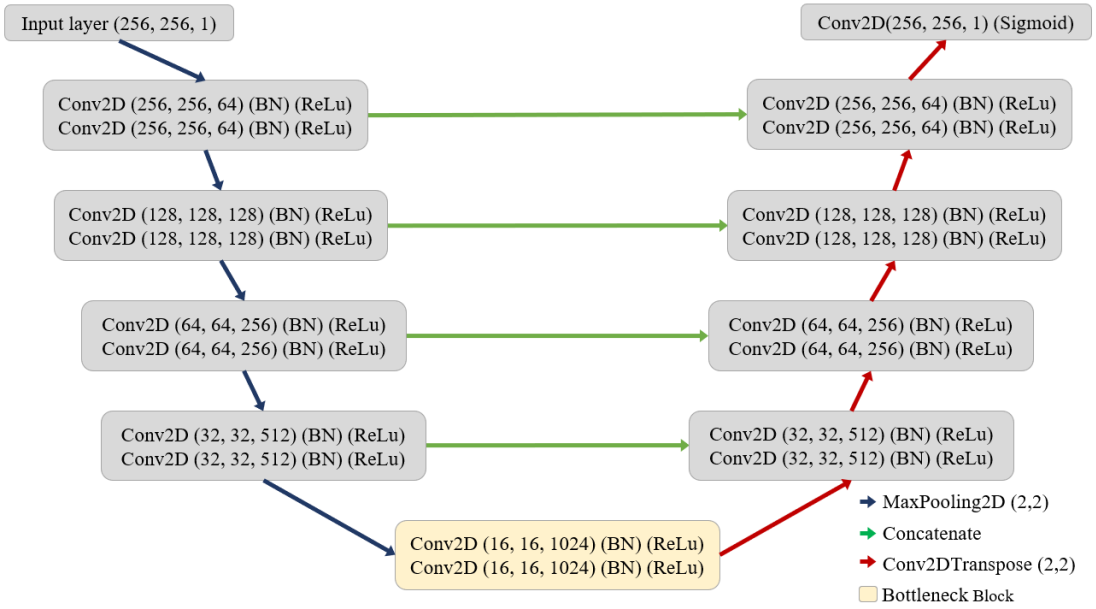

Fig. 4. Model architecture of the proposed neural network.

TABLE I
EVALUATION RESULTS ON THE TWO-PHASE FLOW TEST SET. COMPARISON BETWEEN THREE HOLDOUT PERCENTAGES.

Holdout (%)	Training Time (seg)	Pixel Accuracy (%)	BPA (%)	Mean IoU (%)	DSC
40	125.0±73.4	86.79±10.92	75.39±0.21	64.09±26.91	0.5690±0.3851
30	143.4±59.2	99.79±0.01	99.80±0.00	98.62±00.42	0.9960±0.0002
20	171.4±56.8	**99.81±0.01**	**99.80±0.00**	**99.43±0.06**	**0.9965±0.0001**

segment the region containing the bubble. However, the U-Net in test image #4 is able to accurately segment an image from the test set. The tests with other holdout percentages performed better. As the holdout percentage decreases, both the Mean IoU and the Dice coefficient increase, reaching values of 99.43% and 0.9965, respectively. These results show that the proposed model is robust and reliable.

A complementary visual inspection of the results was also conducted, by randomly selecting two additional images from the test set. Figure 6 shows images of the test set with their respective masks and U-Net predictions. It is possible to observe that the neural network is capable of accurately segmenting asymmetrically shaped bubbles and also in the opposite position in relation to most of the others. Even regions with reflection and presence of particles were correctly segmented.

V. CONCLUSION

In this study we evaluated a semantic segmentation method, i.e. the U-Net neural network architecture, for bubble detection in multiphase flow PIV. For that, we built a new dataset with images and manual annotations of the location of the bubbles, and trained and evaluated the neural network with 1161 images, with varied training-validation partitionings. The results obtained by simply using an off-the-shelf architecture for the task indicates that it is possible to further improve the results presented in many aspects, as the results reached 99.81% and 86.78% of accuracy for 80% and 60% of the images for training, respectively, and we will try to ellaborate next.

The main finding is that the methodology for bubble detection with a reduced number of images is feasible, as it is costly to generate and annotate data in such a setting. By collecting and labeling more training data, it will be possible to handle both the data-hungry requirements of U-Net and have better results in the hold-out phase. Yet, by using transfer learning we will possibly be able to use different experiments from different groups, which possibly might lead to better models in hold-out without necessarily requiring more labeled data. Additionally, we also think that non-semantic, more traditional methods can be used to perform multi-step segmentation, such as by firstly removing the fluid from the background, then applying segmentic segmentation only on the more difficult region containing fluids. By optimizing an architecture such as the U-net, we may obtain better runtime for the architecture and thus enable the velocity field to be used in real-time for feedback by using dedicated hardware with embedded GPUs. The future research directions highlighted is varied and we will tackle some of this issues in forthcoming work toward more rapid, efficient, and accurate PIV for multiphase flow.

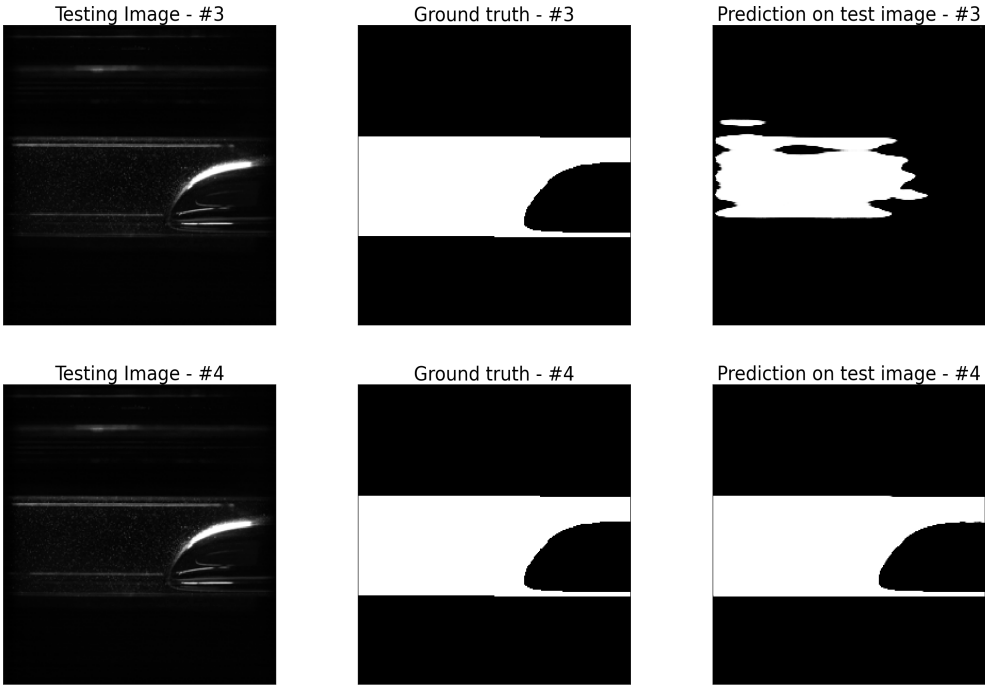

Fig. 5. Result of tests #3 and #4.

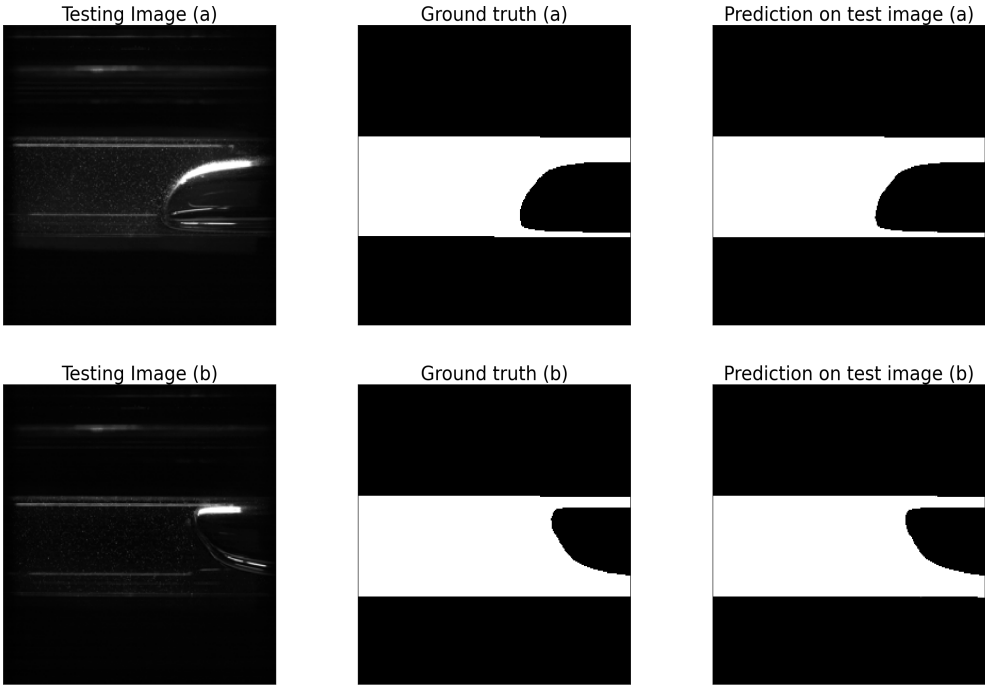

Fig. 6. Result of semantic segmentation of asymmetric bubbles.

The impact of the present work will enable different applications and future research directions. By using such a image processing method for detecting bubbles will imply many benefits, such as (i) performing PIV more accurately and requireing less tedious trial and error tasks for labeling bubbles manually, (ii) performing PIV on real-time, as currently the existing methods fail to deal with both pre-processing for detecting bubbles and assessing particle velocities, to cite a few. With further development of the bubble detection model, by providing an increased training set, optimizing the model architetecture, and enhancing its real-time capabilities, a fully-automated CV-based system for PIV can be built and even be

run online.

REFERENCES

[1] Irfan Khan, Mingjun Wang, Yapei Zhang, Wenxi Tian, Guanghui Su, Suizheng Qiu, "Two-phase bubbly flow simulation using CFD method: A review of models for interfacial forces", Progress in Nuclear Energy, vol. 125, 2020.

[2] Igor Poletaev, Mikhail P. Tokarev, Konstantin S. Pervunin, "Bubble patterns recognition using neural networks: Application to the analysis of a two-phase bubbly jet", International Journal of Multiphase Flow, vol. 126, 2020.

[3] Raffel M, Willert CE, Wereley ST, Kompenhans J, "Particle image velocimetry", 2nd ed. Springer, Berlin, pp 241–258, 2007.

[4] R.F.L. Cerqueira, E.E. Paladino, B.K. Ynumaru, C.R. Maliska, "Image processing techniques for the measurement of two-phase bubbly pipe flows using particle image and tracking velocimetry (PIV/PTV)", Chemical Engineering Science, vol. 189, pp. 1-23, 2018.

[5] Baojie Liu, Xiaobin Xu, Xianjun Yu, Guangfeng An, "Method for utilizing PIV to investigate high curvature and acceleration boundary layer flows around the compressor blade leading edge", Chinese Journal of Aeronautics, vol. 35,pp. 72-88, 2022.

[6] Zhu, L.-T., Chen, X.-Z., Ouyang, B., Yan, W.-C., Lei, H., Chen, Z., Luo, Z.-H. "Review of machine learning for hydrodynamics, transport, and reactions in multiphase flows and reactors". Industrial and Engineering Chemistry Research, 61, pp. 9901– 9949, 2022.

[7] Oh, J.S., Lee, H. and Hwang, W. "Motion blur treatment utilizing deep learning for time-resolved particle image velocimetry", Experiments in Fluids 62, 234, 2021.

[8] Goldshmid, R.H., Winiarska, E. and Liberzon, D., "Next generation combined sonic-hotfilm anemometer: wind alignment and automated calibration procedure using deep learning", Experiments in Fluids 63, 30, 2022.

[9] Raibaudo, C., Martinuzzi, R.J. "Unsteady actuation and feedback control of the experimental fluidic pinball using genetic programming", Experiments in Fluids 62, 219, 2021.

[10] Prajwal Bhattarai, Szymon Krupiński, Vikram Unnithan, Francesco Maurelli, Nicola Secciani, Matteo Franchi, Alessandro Ridolfi, Leonardo Zacchini, "A Deep Learning Approach for Underwater Bubble Detection", OCEANS, pp. 1-5, 2021.

[11] Redmon, Joseph and Farhadi, Ali, "YOLOv3: An Incremental Improvement", arXiv:1804.02767v1, 2018.

[12] Arif Rokoni, Lige Zhang, Tejaswi Soori, Han Hu, Teresa Wu, Ying Sun, "Learning new physical descriptors from reduced-order analysis of bubble dynamics in boiling heat transfer", International Journal of Heat and Mass Transfer, vol. 186, 2022.

[13] Kim, Y., Park, H. "Deep learning-based automated and universal bubble detection and mask extraction in complex two-phase flows", Scientific Reports, 11, 8940, 2021.

[14] Choi, D., Kim, H. and Park, H., "Bubble velocimetry using the conventional and CNN-based optical flow algorithms", Scientific Reports, 12, 2022.

[15] Hendrik Hessenkemper, Sebastian Starke, Yazan Atassi, Thomas Ziegenhein, Dirk Lucas, "Bubble identification from images with machine learning methods", arXiv:2202.03107, 2022.

[16] G. Zhou and A. Prosperetti, "Faster Taylor bubbles," Journal of Fluid Mechanics, vol. 920, p. R2, 2021.

[17] Yuguo Zhou, Yanbo Ren, Erya Xu, Shiliang Liu, Lijian Zhou, "Supervised semantic segmentation based on deep learning: a survey", Multimedia Tools and Applications 81, pp. 29283–29304, 2022.

[18] Fahimeh Fooladgar, Shohreh Kasaei, "A survey on indoor RGB-D semantic segmentation: from hand-crafted features to deep convolutional neural networks", Multimedia Tools and Applications 79, pp. 4499–4524, 2020.

[19] F. Lateef, Y. Ruichek, "Survey on semantic segmentation using deep learning techniques", Neurocomputing, 338 , pp. 321-348, 2019.

[20] Ronneberger, O., Fischer, P., Brox, T., "U-Net: Convolutional Networks for Biomedical Image Segmentation". In: Navab, N., Hornegger, J., Wells, W., Frangi, A. (eds) Medical Image Computing and Computer-Assisted Intervention – MICCAI 2015. MICCAI 2015. Lecture Notes in Computer Science, vol. 9351. Springer, Cham., 2015.